

Ubiquitous Superconducting Diode Effect in Superconductor Thin Films

Yasen Hou^{1*}, Fabrizio Nichele², Hang Chi^{1,3}, Alessandro Lodesani¹, Yingying Wu¹, Markus F. Ritter², Daniel Z. Haxell², Margarita Davydova⁴, Stefan Ilić⁵, Ourania Glezakou-Elbert⁶, Amith Varambally⁷, F. Sebastian Bergeret^{5,8}, Akashdeep Kamra^{9*}, Liang Fu⁴, Patrick A. Lee^{4*}, Jagadeesh S. Moodera^{1,4*}

¹*Francis Bitter Magnet Laboratory and Plasma Science and Fusion Center, Massachusetts Institute of Technology, Cambridge, MA 02139, USA*

²*IBM Research Europe - Zurich, Säumerstrasse 4, 8803 Rüschlikon, Switzerland*

³*U.S. Army CCDC Army Research Laboratory, Adelphi, Maryland 20783, USA*

⁴*Department of Physics, Massachusetts Institute of Technology, Cambridge, MA 02139, USA*

⁵*Centro de Física de Materiales (CFM-MPC), Centro Mixto CSIC-UPV/EHU, Pº Manuel de Lardizabal 5, Donostia-San Sebastián 20018, Spain*

⁶*Hanford High School, Richland, Washington 99354, USA*

⁷*Vestavia Hills High School, Vestavia Hills, Alabama 35216, USA*

⁸*Donostia International Physics Center (DIPC), Donostia-San Sebastián 20018, Spain*

⁹*Condensed Matter Physics Center (IFIMAC) and Departamento de Física Teórica de la Materia Condensada, Universidad Autónoma de Madrid, E-28049 Madrid, Spain*

* Corresponding authors. Email: yshou@mit.edu (Yasen Hou); akashdeep.kamra@uam.es (Akashdeep Kamra); palee@mit.edu (Patrick A. Lee); moodera@mit.edu (Jagadeesh S. Moodera)

ABSTRACT

A superconductor exhibiting a polarity-dependent critical current is of fundamental as well as technological interest, because the superconducting (SC) layer can then admit a perfect dissipationless transmission along one direction while offering a large resistance along the opposite, leading to a phenomenon called SC diode effect or rectification. Here we demonstrate that SC diode effects are ubiquitous in superconductors and observable in a large variety of settings. Controllable via an out-of-plane magnetic field, we observe an extremely sensitive SC diode effect (type A) in superconducting vanadium or niobium stripes with symmetry breaking between their two edges. Nonreciprocity of critical current results from an out-of-plane field as small as 1 Oe, while the diode efficiency and polarity are manipulated

via the strength and direction of the field. With the out-of-plane field carefully eliminated, an in-plane field also creates a sizeable asymmetry between critical currents (type B), regardless of whether this field is perpendicular or parallel to the current flow direction. Finally, we demonstrate nonreciprocal critical currents with a giant diode efficiency reaching 65% when the SC V film couples to a ferromagnetic EuS layer with in-plane magnetization orthogonal to current flow (type C) and a clear diode rectification is seen. This is also realized at zero applied field, in the remnant magnetic state of EuS. Our observations show the ubiquity of the superconducting diode effect. Providing valuable guidance, they demonstrate the need for careful sample design for employing SC diode effect as a mean to study exotic superconducting state, which becomes feasible only when intrinsic pair breaking determines the critical current. Our work paves the way for the development of versatile SC rectifiers employing simple structures using widely available materials.

One-Sentence Summary: Superconductivity

Introduction

Similar to a traditional semiconductor diode, a superconductor with non-reciprocal current flow, a SC diode, may form the building block for, e.g., dissipationless SC digital logic. The recent observation of such a SC diode effect in a complex thin film superconductor heterostructure subjected to an external magnetic field has stimulated vigorous activity towards understanding and replicating it (1). Supercurrent rectification has also been demonstrated in multiple Josephson junction systems including Al-InGaAs/InAs-Al (2), NbSe₂/Nb₃Br₈/NbSe₂ (3) and Nb-NiTe₂-Nb (4), where largest nonreciprocities are observed at large in-plane magnetic fields (2, 4). Furthermore, an intrinsic SC diode effect has been observed in few-layer NbSe₂ (5) and twisted trilayer graphene/WTe₂ heterostructures (6) in an out-of-plane magnetic field. To quantify the diode effect, it is common to introduce an asymmetry parameter, called the diode efficiency, $\eta = \frac{I_c^+ - I_c^-}{I_c^+ + I_c^-}$ where I_c^+ and I_c^- are the critical currents in the two directions. The value of η denotes the magnitude of the

diode effect, while the sign defines the polarity. Up to now, reported values of η range from a few percent to 30% (1-6).

Several theoretical mechanisms have been proposed to explain the SC diode effects in superconductors (7-10) and in Josephson junctions (11, 12), with special emphasis on a potential role of the finite-momentum pairing (7-12). The breaking of time-reversal and inversion symmetries in a superconductor with Rashba spin-orbit coupling (SOC) supports a helical superconducting phase, with the order parameter modulated in a direction transverse to the Zeeman field: $\Delta(r) = \Delta e^{iq_0 r}$. In such a finite-momentum pairing mechanism, Cooper pairs gain a finite momentum q_0 , and the depairing effect for supercurrents flowing parallel and anti-parallel to q_0 is different, leading to a critical current nonreciprocity. On general grounds, interfaces cause inversion symmetry-breaking and Rashba SOC along the normal z direction thereby admitting a polar and odd-under-time-reversal vector T along $z \times h$, where h is an applied magnetic field or an exchange field induced by an adjacent ferromagnet (FM) (13). Thus, application of an in-plane magnetic field perpendicular to the current flow direction should activate T , resulting in peculiar superfluid condensate properties and a critical current nonreciprocity.

The exotic finite-momentum pairing mechanism focuses on the intrinsic depairing current (7-12). However, it is known that nearly all of the superconductor films fail to be governed by the critical pair breaking mechanism, which merely offers the theoretical maximum for a specially designed sample (14-16). A broad range of other mechanisms come to govern different samples (17, 18). Magnetic flux, or Abrikosov vortices, are normally pinned to defect centers or surface barrier of a superconductor (19). The current flow, however, produce a Lorentz force on the vortices. A critical current is often measured when the pinning centers or the surface barrier cannot hold vortices anymore and dissipation starts in the superconductor (13, 18, 20). This principle has been exploited to engineer superconducting vortices-based rectifiers (21-25). Furthermore, Vodolazov and Peeters predicted existence and engineering of SC diode effect employing controlled edge disorder (21). This escaped experimental realization thus far and the present work accomplishes it.

In the present work, using V and Nb superconductors, we demonstrate three types of the SC diode effect rooted in Meissner screening instead of the relatively rare finite-momentum pairing. We first demonstrate nonreciprocal critical current I_c in a superconductor film which is sensitively dependent on the out-of-plane magnetic field: a noticeable SC diode effect (type A) is enabled by a magnetic field as small as 1 Oe. Then, by eliminating the out-of-plane magnetic field carefully, critical current nonreciprocity (type B) is observed with an in-plane magnetic field independent of its orientation with respect to the current flow direction. Furthermore, for a superconductor adjacent to a ferromagnetic layer, a large diode effect (type C) with efficiency $\sim 65\%$ is demonstrated. Physical mechanisms underlying each of the three types of nonreciprocities are discussed and approaches for further enhancing the diode efficiency are proposed. The ubiquity of the diode effect in superconducting films and their heterostructures implies that careful checks with control heterostructures as done in this paper are necessary before claims of novel mechanism can be considered to be established. Furthermore, our work demonstrates a robust control of the nonreciprocity in the simplest conventional superconductors and their hybrids without requiring any SOC or complex structures. Our demonstrated diode efficiencies are the highest reported thus far.

Results

Section 1: Type A – Out-of-plane field induced diode effect in SC thin films.

The V, Nb and EuS films in our experiments were deposited on clean, heated sapphire substrates in a single deposition process in a molecular-beam epitaxy (MBE) chamber with a base pressure of less than 4×10^{-10} Torr. The typical thickness d_m of EuS was 5 nm while the V (or Nb) thickness d was 8 nm. The film was then patterned by electron beam lithography and Ar ion milling into a Hall bar geometry, with width $W \sim 8 \mu\text{m}$ and length $L \sim 48 \mu\text{m}$ (Fig. 1A). A typical V device has a T_c of 3.5 K \sim 4.3 K and a residual resistance ratio around 3 (fig. S1). Current vs voltage scans were recorded in a four-probe geometry to observe the critical current nonreciprocity. The I - V scans taken at 1.8 K for a single layer V film subjected to out-of-plane magnetic field are shown in Fig. 1B. In each scan, increasing and decreasing current sweeps

showed distinct critical current values: a critical current I_c^\pm was observed marking the SC to normal state transition, whereas a much smaller retrapping current I_r^\pm was recorded while transitioning from the normal to the SC state. The low I_r^\pm is often attributed to self-heating when the film is in the normal state (3, 4). In this study, we focus on I_c^\pm where the nonreciprocity was found to be controllable by applying an out-of-plane magnetic field. With 2.8 Oe field applied along the $+z$ direction, critical current for positive current direction (I_c^+) was significantly larger than when the current flow was in the reverse direction (I_c^-). Flipping the magnetic field to $-z$ direction interchanged the magnitudes of I_c^+ and I_c^- . The magnetic field dependence of the effect is plotted in Fig. 1C. We found I_c to show extreme sensitivity to the applied field. A noticeable current rectification even occurs with less than 1 Oe applied field, whereas its polarity could be controlled by the applied field direction. The changes of both I_c^+ and I_c^- as a function of field follow an “inverted V” shape, the peaks occurring at ± 2.45 Oe. The diode efficiency plotted against the magnetic field in Fig. 1D exhibits a maximum efficiency of $\sim 19\%$ seen at ± 2.8 Oe. Such supercurrent rectification (type A) was observed in all the superconducting devices we measured. I - V scans of another V device and a Nb device are presented in fig. S2, showing similar nonreciprocity in critical current controlled by an out-of-plane magnetic field.

The critical current nonreciprocity is not expected without breaking the mirror symmetry with respect to the x - z plane, as the $+x$ and $-x$ directions are equivalent. Thus, we attribute the observed diode effect to a combination of Meissner current generated to screen the applied magnetic field and symmetry breaking between the device edges during fabrication. In practice, the two edges of a SC stripe could never be identical, thereby admitting slightly different critical current densities j_c and $j_c + \delta j_c$, both are smaller than the Ginzburg-Landau depairing limit j_{GL} , as indicated in Fig. 1F. When current density in the device is above j_c , the Lorentz force on vortices nucleated at the edge overcomes the Bean-Livingston barrier thereby enabling vortex flow through the sample which destroys superconductivity (20, 21, 26-28). The Meissner effect induces two dissipationless counter-flowing screening current densities $\pm j(B_z)$ at the two edges, when an out-of-plane field is applied. This current flow adds or subtracts to the applied current at opposite edges,

and modifies the measured critical current density values j_c^+ and j_c^- . At small fields, the screening current density is simply the Meissner response $j(B_z) = aB_z$ which is linear with the applied magnetic field, where a is a constant. For the case shown in Fig. 1F, on the $B_z > 0$ side, we have:

$$j_c^+ = j_c + aB_z, \quad j_c^- = j_c - aB_z, \quad \text{when } aB_z < \frac{\delta j_c}{2} \quad (1)$$

$$j_c^+ = j_c + \delta j_c - aB_z, \quad j_c^- = j_c - aB_z, \quad \text{when } aB_z \geq \frac{\delta j_c}{2} \quad (2)$$

Similar results are obtained when the field is pointing in the $-z$ direction. The measured critical currents are $I_c^\pm = Sj_c^\pm$, where S is the cross-section of the device.

$$I_c^+ = S(j_c + aB_z), \quad I_c^- = S(j_c - aB_z), \quad \text{when } aB_z < \frac{\delta j_c}{2} \quad (3)$$

$$I_c^+ = S(j_c + \delta j_c - aB_z), \quad I_c^- = S(j_c - aB_z), \quad \text{when } aB_z \geq \frac{\delta j_c}{2} \quad (4)$$

A fitting with $Sj_c = 3.14 \text{ mA}$, $S\delta j_c = 1.35 \text{ mA}$ and $Sa = 0.275 \text{ mA Oe}^{-1}$ is shown by the black dashed curves in Fig. 1C, which is in very good agreement with the experimental results. As the field increases, an apparent weakening of the Meissner response results in a sublinear dependence of I_c on B . The latter is understood as follows (13). Due to weak but finite bulk pinning, the critical current is determined by the bulk pinning (instead of the surfaces) when the surface barriers have been made smaller than the bulk pinning by the applied magnetic field. When this happens at a field estimated below, the critical current deviates from its linear dependence, the latter resulting from the edges/surfaces playing the main role. This is also the reason for the superconducting diode effect to be decreasing after some field is applied. The critical current is then determined by the bulk pinning (and not the surfaces) and the inversion symmetry breaking due to surfaces starts to be irrelevant. We note here that self-field produced by the current flow is on the order of 10^{-5} Oe and is negligible. It is convenient to define $B_s = j_c/a$ as the field scale where the critical current vanishes, assuming a linear extrapolation. Our fitting parameters yield $B_s = 11.4 \text{ Oe}$. Such a drastic suppression of the critical current by out-of-plane magnetic field in the thin film geometry could be understood by ineffective Meissner screening(29). The physical interpretation is that, in a thin film, the screening current is confined to the plane and is not effective in screening the external

magnetic field. As a result, the field penetrates on the scale of the Pearl length (30) $\lambda_p = 2\lambda^2/d \gg \lambda$. Maksimova (29) considered the case $\lambda < W < \lambda_p$ and found that $B_s = \phi_0/(\sqrt{3}\pi \xi W)$, where ξ is the coherence length. For $W > \lambda_p$ we replace W by $2\lambda_p$ in this formula (Supplementary Note 1). For V we estimate that $\lambda = 130$ nm and $\lambda_p = 4.25$ μ m, which is somewhat smaller than $W = 8$ μ m. Using $\xi = 11$ nm (fig. S3), we obtain a rough estimate of $B_s \sim 40$ Oe which is larger than the observed value, but is of comparable scale.

As the peak diode efficiency is determined by the edge asymmetry, we fabricated devices with and without a lithographically defined edge asymmetry (serrated edge) on the film from the same growth. Critical current vs magnetic field for both devices are shown in fig. S4. The device without defined asymmetry shows a peak value for diode efficiency of 21%, while the one with a serrated edge attains a much larger diode efficiency, reaching ~50%. Critical current peaks of the device with defined asymmetry occur at ± 5.1 Oe, much larger than 1.5 Oe for the device without it, which shows (and agrees with) a larger δj_c between the edges. As temperature increases, both critical currents and diode efficiency drop (fig. S5). These results provide further evidence for the Meissner screening mechanism and a practical approach to enhance the diode efficiency (21).

Experimentally, a drastic suppression of the critical current by an out-of-plane field has been reported in other superconductor films such as NbN (31), TaN (31), MgB₂ (32), (Li,Fe)OHFeSe (33) and Nb/SrRuO₃ bilayers (34). However, no asymmetrical critical currents were reported except for a recent work on grainy Sn films which was largely unnoticed by the community (35).

Section 2: Type B - In-plane field induced diode effect in SC thin films.

Due to the highly sensitive dependence of the critical current on the out-of-plane field, a false “in-plane” magnetic field induced diode effect could easily be measured. In our study, the device was mounted on a rotating sample holder in a DynaCool Physical Property Measurement System (PPMS) set up, with a minimum step rotation of 0.01°. The thin film was mounted so that the in-plane magnetic field was along the y axis ($\theta = 0^\circ$). The red curve in Fig. 1E shows the I - V scans of the device with a 2 T “in-plane” applied magnetic field showing different I_c^+ and I_c^- values suggesting a SC diode effect. However, when the device

was rotated to $\theta = -0.01^\circ$, the asymmetry of I_c^+ and I_c^- was reversed. With such a small rotation, the change of the in-plane component of the magnetic field was $\sim 3 \times 10^{-4}$ Oe, which is too small to have any effect on the device. Thus, we attribute the apparent in-plane diode effect in Fig. 1E to the residual out-of-plane component of the magnetic field. Limited by the resolution of the rotator, the magnetic field was only nominally along the y axis and the offset angle could easily be somewhere between -0.01° to 0.01° . The corresponding out-of-plane component of the magnetic field B_z was up to 3.5 Oe when a 2 T field was applied to observe an apparent in-plane diode effect. The polarity reversal of the nonreciprocity can then be due to a change in the B_z component. In our study, the angle between the magnetic field and the film plane was carefully calibrated so that residual offset angle was only limited by the equipment resolution. Without calibration, we found that the offset angle could be anywhere from -1° to 1° , when manually placing the device along a certain plane. In this case, the false in-plane field-induced diode effect occurs even when the applied field is as small as 100 Oe. Because of this observation, we believe that while investigating the SC diode effect under an in-plane magnetic field, any out-of-plane component of the field needs to be taken into consideration and carefully removed.

To study the effects of the real in-plane magnetic field on the critical currents, we developed a technique that enables us to remove the out-of-plane field up to an accuracy of < 0.1 Oe (Supplementary Note 2). Fig. 2A presents I_c^\pm and $|\eta|$ vs the actual in-plane magnetic field along the y axis (perpendicular to the current flow). A clear critical current rectification (type B) occurred with the applied field, where the diode polarity was controlled by the field direction. Diode efficiency was found to increase linearly with the in-plane field, although it remained significantly smaller than in the type A configuration.

To gain further insight into the origin of in-plane field induced diode effect, we performed critical current measurements when the field was parallel to the current flow and the results are plotted in Fig. 2B. Our results show that the behavior of I_c^\pm and η with the in-plane field parallel to the current flow is very similar to the case of perpendicular to the current flow. A diode effect is not expected when the field is strictly in-plane and parallel to the current flow because the screening current is perpendicular to the applied current.

Thus, we note here that the physical origin for type B diode effect remains unclear and encourages further exploration.

Section 3: Type C - In-plane field induced diode effect in SC/FM heterostructures

We investigated furthermore the critical current rectification of the third kind (type C) in a hybrid structure where the superconductor film has a ferromagnetic layer over it. Recent studies proposed to combine the Rashba SOC on the surface of the superconductor subjected to spin-splitting field \hbar caused by a magnetic field or via exchange interaction with a FM. Variants of this proposal have recently been realized in a Josephson tunnel junction geometry (2-4). The suggestion was to realize this scenario by sandwiching a SC layer between a FM insulator and a heavy metal to provide the Rashba SOC, and thus creating the needed top/bottom asymmetry (8, 9). Inspired by this proposal, we fabricated such a trilayer system, Pt(1Å)/V/EuS and observed a giant SC diode effect. Fig. 3A shows the I - V scans of a Pt/V/EuS trilayer when the EuS layer was magnetized along the y direction (in-plane and perpendicular to the current flow). With a small external field to magnetize the EuS layer, a dramatic difference was observed between the critical current along the positive and negative directions of current flow. At $B_y = -30$ Oe, I_c^+ was more than 4 times larger than I_c^- , producing a giant critical current ratio of 480% and a diode efficiency of 65%, the highest value of diode rectification seen in superconductors as yet. The critical current asymmetry was reversed when the EuS magnetization direction was flipped. The temperature, magnetic field and angle dependencies of the SC diode effect were systematically studied on a second Pt/V/EuS device. A clear supercurrent rectification is also demonstrated in fig. S8. As the temperature increased, I_c^+ and I_c^- reduced whereas η remained nearly unchanged from 60 mK up to 1.3 K (Fig. 3B). Further increase of the temperature led to a significant drop of I_c^+ , I_c^- and η , although clear diode phenomenon was seen even up to 3.6 K, close to T_c . At 1 K, the effect was found to quickly reach a maximum value as the field was increased to 18 Oe (Fig. 3C), and beyond that the magnitude of I_c^+ , I_c^- , and η decreased slightly as the field increased. Hysteresis in the critical currents and diode efficiency was observed which resembled the magnetic hysteresis of the EuS film. This hysteresis in I_c enables control of the diode polarity via the

remnant EuS magnetization direction, for field free scenario. Diode efficiency at zero external field, though a little smaller than the maximum value when EuS is fully magnetized, was still 21% for the Pt/V/EuS device. The nonreciprocity sensitively depended on the angle between the magnetic field and the current flow direction. Fig. 3D shows diode efficiency on a polar plot. The largest asymmetry was observed when the magnetic field was perpendicular to the current flow direction, while it was negligible when the field was parallel to the current flow.

It is tempting to interpret the giant supercurrent rectification in Pt/V/EuS as support for the finite-momentum pairing mechanism with Pt providing the required Rashba SOC and exchange coupling with EuS giving a large spin-splitting in the V layer. However, upon further investigations, we discovered that a similarly large nonreciprocity could be observed in a V/EuS bilayer device, without Pt providing the Rashba SOC (Fig. 3E). Temperature (Fig. 3F), magnetic field and angle (fig. S9) dependencies of the SC diode effect were systematically measured on a second V/EuS device, all show close resemblance to the Pt/V/EuS case. Moreover, Fig. 3, G and H show similar EuS-magnetization-controlled diode effect in Nb/EuS bilayers, and persisting up to 6.5 K, as the T_c for Nb was higher compared to that of V (Fig. 4A).

There remains the possibility that Rashba SOC comes from the interface with EuS. To test this hypothesis and further examine the role of the exchange field, we fabricated Nb/EuS and Nb/Al₂O₃/EuS films in one deposition cycle. Two substrates were placed on the sample holder and a mask was used to cover one of them during the deposition of the 3 nm-thick Al₂O₃ film that serves as a spacer layer. Without direct contact with the ferromagnetic layer, the Nb/Al₂O₃/EuS trilayer showed a slightly lower resistance and a higher T_c (4a). *I-V* scans at 1.8 K showed that both films had very similar critical currents when EuS was magnetized along the same direction (Fig. 4, B and C). The observed critical current nonreciprocity in Nb/Al₂O₃/EuS trilayer, comparable to Nb/EuS bilayer, indicates that a direct contact between the SC and FM layer was not required for type C diode effect. Based on these observations, we conclude that neither Rashba SOC nor interfacial exchange with the FM are essential in the observed I_c nonreciprocity. Thus, we can rule out the finite-momentum pairing mechanism as the underlying cause of our observed diode effects.

The diode effect in SC/FM bilayers has been reported in other systems (36) including LSMO/YBCO (37), Nb/Co (27, 38) and Py/Nb (39, 40) heterostructures. The phenomenon could be understood by a screening current mechanism (27) shown schematically in Fig. 4D. The in-plane magnetization along the y axis of the FM layer produces oppositely oriented fringing magnetic fields in the y - z plane at the two edges. A calculation shows that, for distances r larger than the film thickness d_m , the fringing field can be viewed as emerging radially from point sources with opposite signs at the opposite edges and decay as $1/r$ (41). This produces a z component of the magnetic field given by:

$$B_z = 2md_m z / (z^2 + y^2) \quad (5)$$

where z and y are measured from the sample edges and m is the magnetization density. For EuS, we assume the Eu moment is saturated at $\mu_s = 7\mu_B$ and estimate $4\pi m \sim 1.5$ T (42). Similar to the type A configuration, this perpendicular magnetic field produces a Meissner screening current flowing in the $+x$ direction. However, there are two important differences. Since the fringing field reverses direction on the two edges, the current on both edges now flows in the same direction (Fig. 4D), and a diode effect can take place without requiring edge asymmetry as in type A. This current flow adds to the external current in the $+x$ direction, but partly cancels the external current in $-x$ direction, resulting in a smaller I_c^+ and larger I_c^- . By reversing the magnetization of the EuS layer, screening current flows to the $-x$ direction, which reverses the diode current polarity. A second difference is that, unlike a uniform applied magnetic field, the fringing fields are strongly localized near the edges. The magnitude of the screening current is estimated using the London equation. The x component of the vector potential is obtained by integrating $\mathbf{B} = \nabla \times \mathbf{A}$, i.e., $B_z = \frac{\partial A_x}{\partial y}$. In the London gauge we find:

$$A_x(y) = \int_0^y B_z(z, y') dy' \quad (6)$$

where we have shifted the y coordinate so that the sample lies between $y = -W/2$ and $W/2$. Using equation (5) in the shifted coordinate, we find that right at the sample edge, the A_x field is independent of z and is given by $A_x = \pi m d_m$. From the edge it extends into the sample by a distance $\sim d$ in the y direction. Using the London equation $j_x = \frac{c}{4\pi} \frac{A_x}{\lambda^2}$, we find that, at the sample edge, the current is given by:

$$j_0 = \frac{c}{4\pi} \frac{\pi m d_m}{\lambda^2} \quad (7)$$

On the other hand, the critical current density of the SC film is estimated by the GL theory as:

$$j_{GL} = \frac{c}{4\pi} \frac{\phi_0}{3\sqrt{3}\pi\xi\lambda^2} \quad (8)$$

The ratio between the screening current density and the critical current density is then:

$$\frac{j_0}{j_{GL}} = \frac{3\sqrt{3}\pi^2 m d_m \xi(T)}{\phi_0} \quad (9)$$

By using $4\pi m = 1.5T$, $d_m = 5nm$, $\xi = 12nm$, $\phi_0 = 2 \times 10^3 T(nm)^2$, we estimate:

$$\frac{j_0}{j_{GL}} = 0.17 \quad (10)$$

This rough estimate shows that the screening current due to the fringing field is comparable to the critical current and can lead to diode effect. It is worth noting that the size of this ratio benefitted from the large numerical factor in the denominator in equation (8) for j_{GL} . The ratio is proportional the thickness of the FM film and can be increased using thick films, keeping in mind that the estimate is valid only for $d_m < d$. Once the screening current exceeds the critical current at the edge, we adopt the commonly used picture that vortices start to enter and flow across the samples, leading to a resistive state.

Conclusion

In summary, we demonstrated three types of the superconducting diode effect, of which two are rooted in the universal Meissner screening. Two of these types, A and B, employ isolated superconductor films and are controlled by applied magnetic fields. While the third type C exists in superconductor/ferromagnet hybrids, and enables a nonvolatile control via the ferromagnet magnetization. The ubiquitous nature of the phenomena implies that these contributions exist in all similar devices, without the need for spin-orbit or direct exchange coupling, and thus without having to invoke an exotic superconducting state. Our extensive control experiments taking all precautions to investigate in various configurations (with and without inversion symmetry and time reversal symmetry broken) show the universality of the SC diode phenomena. Hence, studying a potential finite momentum paired superconducting order in a film via critical current nonreciprocity can only be accomplished via a careful device design that eliminates the role of vortices in

determining the critical current, and as a result achieves the pair breaking mechanism. From the point of technology development, we demonstrated a giant diode efficiency of 65% using a 30 Oe external magnetic field and a field-free nonvolatile diode effect with an efficiency of 21%, settings the stage for envisioning computation architectures based on superconducting rectification.

References

1. F. Ando *et al.*, Observation of superconducting diode effect. *Nature* **584**, 373-376 (2020).
2. C. Baumgartner *et al.*, Supercurrent rectification and magnetochiral effects in symmetric Josephson junctions. *Nat. Nanotechnol.* **17**, 39-44 (2022).
3. H. Wu *et al.*, The field-free Josephson diode in a van der Waals heterostructure. *Nature* **604**, 653-656 (2022).
4. B. Pal *et al.*, Josephson diode effect from Cooper pair momentum in a topological semimetal. *Nat. Phys.*, (2022).
5. L. Bauriedl *et al.*, Supercurrent diode effect and magnetochiral anisotropy in few-layer NbSe₂. *Nat. Commun.* **13**, 4266 (2022).
6. J.-X. Lin *et al.*, Zero-field superconducting diode effect in small-twist-angle trilayer graphene. *Nat. Phys.*, (2022).
7. A. Daido, Y. Ikeda, Y. Yanase, Intrinsic superconducting diode effect. *Phys. Rev. Lett.* **128**, 037001 (2022).
8. S. Ilić, F. S. Bergeret, Theory of the supercurrent diode effect in Rashba superconductors with arbitrary disorder. *Phys. Rev. Lett.* **128**, 177001 (2022).
9. N. F. Q. Yuan, L. Fu, Supercurrent diode effect and finite-momentum superconductors. *Proc. Natl. Acad. Sci.* **119**, e2119548119 (2022).
10. J. J. He, Y. Tanaka, N. Nagaosa, A phenomenological theory of superconductor diodes. *New J. Phys.* **24**, 053014 (2022).
11. M. Davydova, S. Prembabu, L. Fu, Universal Josephson diode effect. *Sci. Adv.* **8**, eabo0309 (2022).
12. Yukio Tanaka, Bo Lu, N. Nagaosa, Theory of diode effect in d-wave superconductor junctions on the surface of topological insulator. *Preprint at <https://doi.org/10.48550/arXiv.2205.13177>*, (2022).
13. M. K. Hope, M. Amundsen, D. Suri, J. S. Moodera, A. Kamra, Interfacial control of vortex-limited critical current in type-II superconductor films. *Phys. Rev. B* **104**, 184512 (2021).
14. K. Xu, P. Cao, J. R. Heath, Achieving the Theoretical Depairing Current Limit in Superconducting Nanomesh Films. *Nano Lett.* **10**, 4206-4210 (2010).
15. C. P. Poole, Handbook of Superconductivity. Academic Press: San Diego, CA, 2000.
16. C. C. Tsuei, J. Mannhart, D. Dimos, Limitations on critical currents in high temperature superconductors. *AIP Conf. Proc.* **182**, 194-205 (1989).
17. K. K. Likharev, Superconducting weak links. *Rev. Mod. Phys.* **51**, 101-159 (1979).
18. V. V. Shmidt, Critical Currents in Superconductors. *Sov. Phys. Uspekhi* **13**, 408-409 (1970).

19. C. P. Bean, J. D. Livingston, Surface Barrier in Type-II Superconductors. *Phys. Rev. Lett.* **12**, 14-16 (1964).
20. V. V. Shmidt, The Critical Current in Superconducting Films. *JETP* **30**, 1137 (1970).
21. D. Y. Vodolazov, F. M. Peeters, Superconducting rectifier based on the asymmetric surface barrier effect. *Phys. Rev. B* **72**, 172508 (2005).
22. C. S. Lee, B. Jankó, I. Derényi, A. L. Barabási, Reducing vortex density in superconductors using the ‘ratchet effect’. *Nature* **400**, 337-340 (1999).
23. J. E. Villegas *et al.*, A Superconducting Reversible Rectifier That Controls the Motion of Magnetic Flux Quanta. *Science* **302**, 1188-1191 (2003).
24. J. E. Villegas, E. M. Gonzalez, M. P. Gonzalez, J. V. Anguita, J. L. Vicent, Experimental ratchet effect in superconducting films with periodic arrays of asymmetric potentials. *Phys. Rev. B* **71**, 024519 (2005).
25. D. Cerbu *et al.*, Vortex ratchet induced by controlled edge roughness. *New J. Phys.* **15**, 063022 (2013).
26. M. Benkraouda, J. R. Clem, Critical current from surface barriers in type-II superconducting strips. *Phys. Rev. B* **58**, 15103-15107 (1998).
27. D. Y. Vodolazov *et al.*, Considerable enhancement of the critical current in a superconducting film by a magnetized magnetic strip. *Phys. Rev. B* **72**, 064509 (2005).
28. M. Kupriyanov, K. Likharev, Effect of an edge barrier on the critical current of superconducting films. *Sov. Phys. Solid State* **16**, (1975).
29. G. M. Maksimova, Mixed state and critical current in narrow semiconducting films. *Phys. Solid State* **40**, 1607-1610 (1998).
30. J. Pearl, Current distribution in superconducting films carrying quantized fluxoids. *Appl. Phys. Lett.* **5**, 65-66 (1964).
31. K. Ilin *et al.*, Critical current of Nb, NbN, and TaN thin-film bridges with and without geometrical nonuniformities in a magnetic field. *Phys. Rev. B* **89**, 184511 (2014).
32. C. B. Eom *et al.*, High critical current density and enhanced irreversibility field in superconducting MgB₂ thin films. *Nature* **411**, 558-560 (2001).
33. J. Hänisch *et al.*, Anisotropy of flux pinning properties in superconducting (Li,Fe)OHFeSe thin films. *Supercond. Sci. Technol.* **33**, 114009 (2020).
34. M. Feigensohn, L. Klein, M. Karpovski, J. W. Reiner, M. R. Beasley, Suppression of the superconducting critical current of Nb in bilayers of Nb / SrRuO₃. *J. Appl. Phys.* **97**, 10J120 (2005).
35. A. G. Sivakov, O. G. Turutanov, A. E. Kolinko, A. S. Pokhila, Spatial characterization of the edge barrier in wide superconducting films. *Low Temp. Phys.* **44**, 226-232 (2018).
36. M. V. Milošević, G. R. Berdiyrov, F. M. Peeters, Mesoscopic Field and Current Compensator Based on a Hybrid Superconductor-Ferromagnet Structure. *Phys. Rev. Lett.* **95**, 147004 (2005).
37. N. Touitou *et al.*, Nonsymmetric current – voltage characteristics in ferromagnet / superconductor thin film structures. *Appl. Phys. Lett.* **85**, 1742-1744 (2004).
38. A. Papon, K. Senapati, Z. H. Barber, Asymmetric critical current of niobium microbridges with ferromagnetic stripe. *Appl. Phys. Lett.* **93**, 172507 (2008).
39. G. Carapella, P. Sabatino, G. Costabile, Asymmetry, bistability, and vortex dynamics in a finite-geometry ferromagnet-superconductor bilayer structure. *Phys. Rev. B* **81**, 054503 (2010).

40. G. Carapella, V. Granata, F. Russo, G. Costabile, Bistable Abrikosov vortex diode made of a Py–Nb ferromagnet-superconductor bilayer structure. *Appl. Phys. Lett.* **94**, 242504 (2009).
41. Y. Liu *et al.*, Semiconductor–ferromagnetic insulator–superconductor nanowires: stray field and exchange field. *Nano Lett.* **20**, 456-462 (2020).
42. A. Svane *et al.*, Electronic structure of Sm and Eu chalcogenides. *Phys. Stat. Sol. (B)* **241**, 3185-3192 (2004).

Acknowledgements

Funding: This work was supported by Office of Naval Research (N00014-20-1-2306), National Science Foundation (NSF-DMR 1700137); Army Research Office (W911NF-20-2-0061, DURIP W911NF-20-1-0074). F.N. MFR, DZH acknowledge support from the European Research Council (grant number 804273). H.C. is sponsored by the Army Research Laboratory under Cooperative Agreement Number W911NF-19-2-0015. S.I. and F.S.B. are supported by European Union’s Horizon 2020 Research and Innovation Framework Programme under Grant No. 800923 (SUPERTED), and the Spanish Ministerio de Ciencia e Innovacion (MICINN) through Project PID2020-114252GB-I00 (SPIRIT). F.S.B. acknowledges financial support by the A. v. Humboldt Foundation. A.K. acknowledges the support by the Spanish Ministry for Science and Innovation – AEI Grant CEX2018-000805-M (through the “Maria de Maeztu” Programme for Units of Excellence in R&D). P.A.L. acknowledges the support by DOE office of Basic Sciences Grant No. DE-FG0203ER46076.

Author contributions: Y.H., J.S.M., L.F., F.S.B., and P.A.L. conceived and designed the study. Y.H. grew the samples and fabricated the devices. Y.H. and F.N. performed the measurements. H.C., A.L., Y.W., M.F.R., and D.Z.H. assisted the measurements. O.G.E. and A.V. fabricated devices with defined edges and performed measurements on the devices. Y.H., A.K., P.A.L., and J.S.M. performed theory modeling. M.D., S.I., F.S.B. and F.L. provided discussion and theoretical support. Y.H., A.K., P.A.L., and J.S.M. wrote the paper with contributions from all authors.

Competing interests: The authors declare no competing interests.

Data and materials availability: Experimental data files are available at.. (will add in later).

Supplementary Materials

Materials and Methods

Supplementary note 1 to 2

Figs. S1 to S9

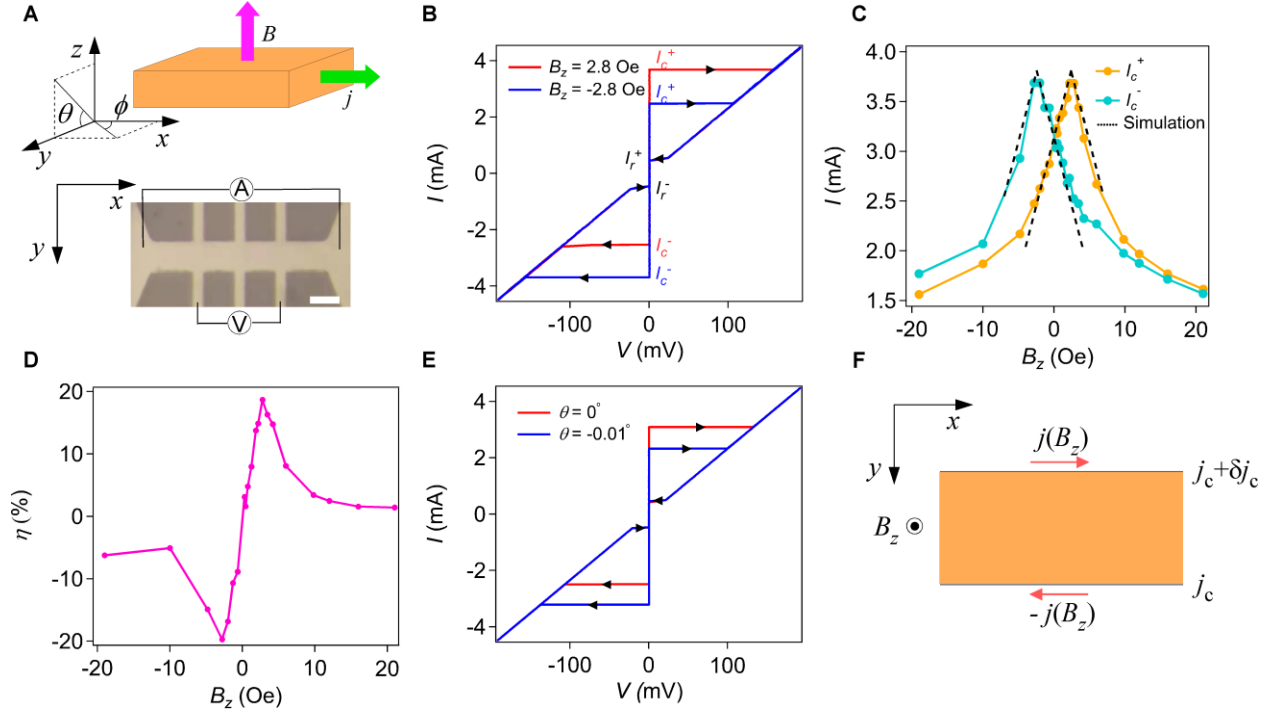


Fig. 1: Demonstration of out-of-plane field induced diode effect in a SC film at 1.8 K. (A) Top: schematic drawing of the vanadium thin film strip. Bottom: optical microscope image of the Hall bar strip of V film. Scale bar denotes $8\mu\text{m}$. (B) I - V scans of the device at 2.8 Oe out-of-plane field along $\pm z$ direction as indicated by the red and blue lines. Black arrows indicate the scan direction. (C) Critical currents as a function of the magnetic field with black dashed line showing the calculated values based on our model. (D) The diode efficiency η vs B_z . (E) I - V scans of the device showing a false “in-plane” diode effect, which is actually caused by the out-of-plane component of the magnetic field. Note the diode polarity is reversed when the magnetic field deviates from nominally in-plane direction by as little as 0.01° . (F) Schematic depiction of Meissner screening currents and the asymmetry between the critical current densities at the two edges.

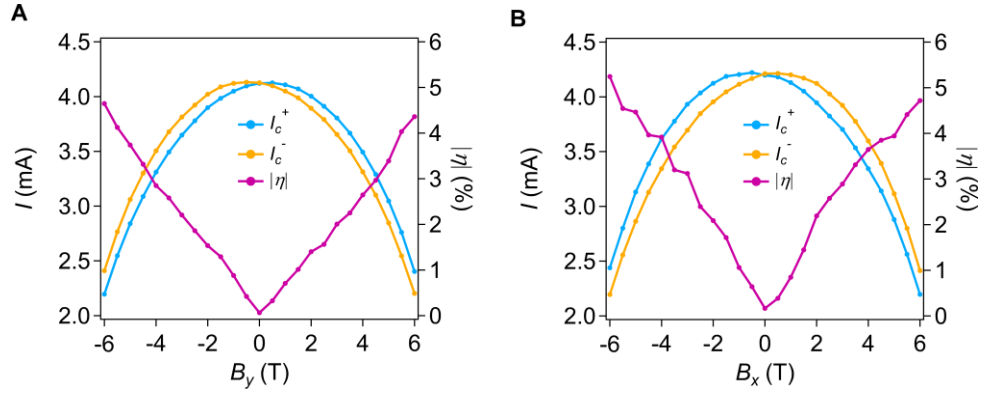


Fig. 2: In-plane field induced SC diode effect in SC V film. (A) I_c^\pm and $|\eta|$ as a function of the in-plane field perpendicular to current flow. (B) I_c^\pm and $|\eta|$ as a function of the in-plane field parallel to current flow. Both sets of data were taken at 500 mK.

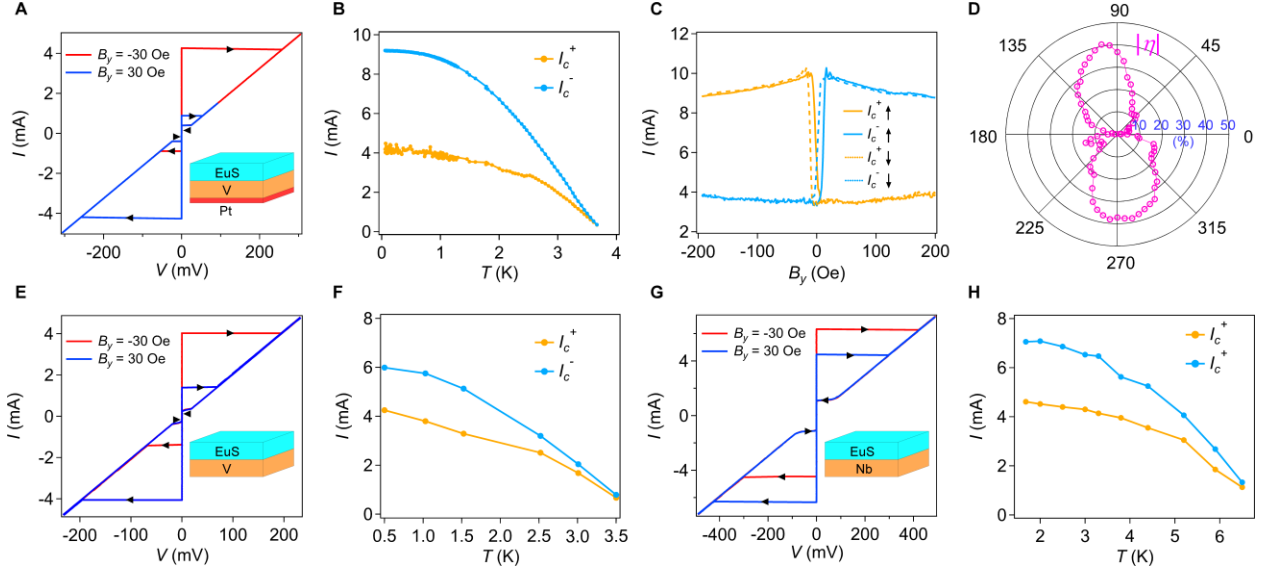


Fig. 3: SC diode effect in SC/FM bilayers. (A) I - V scans of a Pt/V/EuS device showing giant critical current rectification effect at 1.8 K. Inset shows a schematic of the Pt/V/EuS stack. (B) Temperature dependence of the critical current at $B_y = 200$ Oe. (C) Magnetic field dependence of the critical current at 1 K. Solid (dashed) lines were obtained when scanning the magnetic field up (down). (D) Angle (ϕ) dependence of η at $T = 1$ K and $B = 200$ Oe. Data in A and B to D are from two different Pt/V/EuS devices. (E) I - V scans of a V/EuS device showing a similarly large SC diode effect as in Pt/V/EuS. Inset shows a schematic of the V/EuS stack. (F) Temperature dependence of the critical currents for a second V/EuS at $B_y = 30$ Oe. (G) I - V scans of a Nb/EuS device exhibiting the nonreciprocity. Inset shows a schematic of the Nb/EuS stack. (H) Temperature dependence of the critical currents at $B_y = 30$ Oe for the same Nb/EuS device.

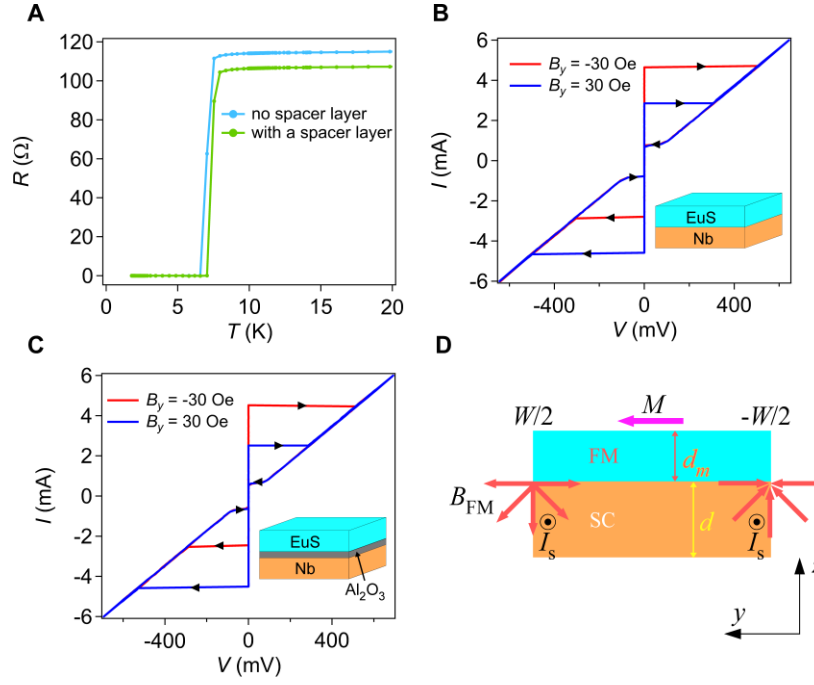


Fig. 4: Screening current mechanism for the SC diode effect in SC/FM bilayers. (A) R - T curves for the SC/FM films with and without a 3 nm Al₂O₃ spacer layer. (B) I - V scans of the Nb/EuS device measured at 1.8 K showing type C SC diode effects. Inset shows a schematic of the Nb/EuS stack. (C) I - V scans of the Nb/Al₂O₃/EuS device at 1.8 K showing similar diode effects as in B. Inset shows a schematic of the Nb/Al₂O₃/EuS stack. (D) Schematic depiction of the screening currents induced by the out-of-plane edge magnetic fields due to the EuS layer. I_s denotes the induced screening current.

SUPPLEMENTARY MATERIALS

for

Ubiquitous Superconducting Diode Effect in Superconductor Thin Films

Yasen Hou^{1*}, Fabrizio Nichele², Hang Chi^{1,3}, Alessandro Lodesani¹, Yingying Wu¹, Markus F. Ritter², Daniel Z. Haxell², Margarita Davydova⁴, Stefan Ilić⁵, Ourania Glezakou-Elbert⁶, Amith Varambally⁷, F. Sebastian Bergeret^{5,8}, Akashdeep Kamra⁹, Liang Fu⁴, Patrick A. Lee^{4*}, Jagadeesh S. Moodera^{1,4*}
* Corresponding authors. Email: yshou@mit.edu (Yasen Hou); akashdeep.kamra@uam.es (Akashdeep Kamra); palee@mit.edu (Patrick A. Lee); moodera@mit.edu (Jagadeesh S. Moodera)

This pdf file includes:

Materials and Methods

Supplementary note 1 to 2

Figs. S1 to S9

Materials and Methods

The growth of V, Nb, EuS, Pt and Al₂O₃ thin films were carried out in a custom-built molecular beam epitaxy system with a base vacuum of $< 4 \times 10^{-10}$ Torr. Polished sapphire Al₂O₃(0001) were used as substrates, whose surface high quality was assured by *ex situ* chemical cleaning and thermal annealing and *in situ* outgassing at 800 °C for 30 min. Subsequently the substrate was cooled down to the growth temperature for growing epitaxial metallic layers. Typical growth temperature was 230°C for V, EuS, Pt and Al₂O₃, and was 500°C for Nb. High-purity V, Nb, Pt and EuS sources were evaporated from an electron-beam source (e-gun) with a growth rate of approximately 0.5 Å/s. The films were patterned to a Hall-bar geometry following standard electron beam lithography and Ar ion milling.

Transport and magnetic measurements were performed in a Quantum Design Physical Property Measurement System (PPMS), equipped with a 9 T superconducting magnet. Current–voltage curves were measured through a current preamplifier (DL Instruments, model 1211), a voltage amplifier (Stanford Research Systems, model SR560) and a National Instruments data acquisition system. Ultra-low temperature transport measurements were performed using advanced electronics and BlueFors dilution fridge fitted with two axes vector magnet.

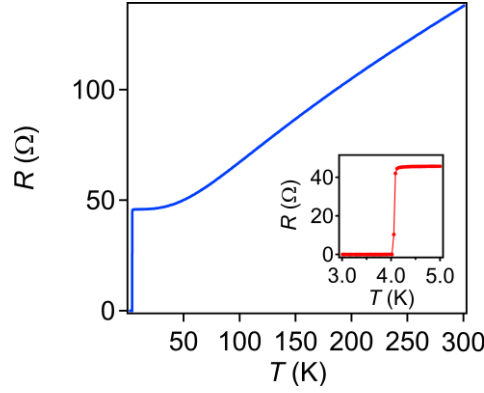


Fig. S1: R - T curve for a typical V device showing $T_c \sim 4.1$ K and a residual resistance ratio ~ 3 .

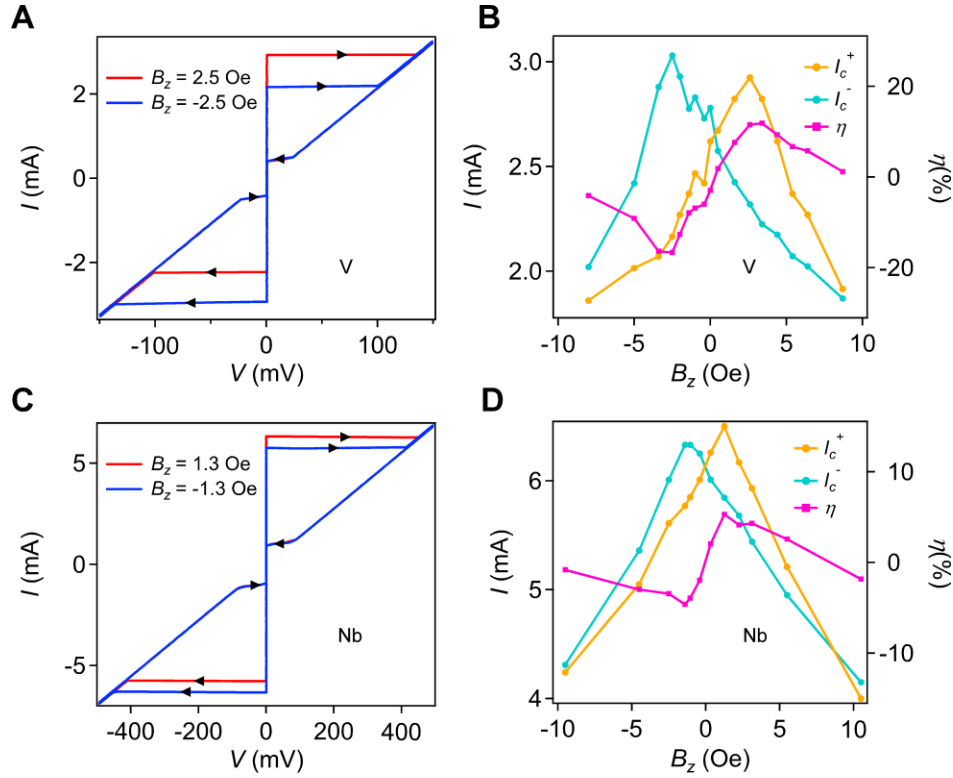


Fig. S2: Type A SC diode effect in another V film and in a Nb film at 1.8 K. (A) I - V scans of a second V device at 2.5 Oe out-of-plane field along $\pm z$ direction as indicated by the red and blue lines. Black arrows indicate the scan direction. (B) Critical currents and diode efficiency as a function of the magnetic field. (C and D) Similar effects in a Nb device.

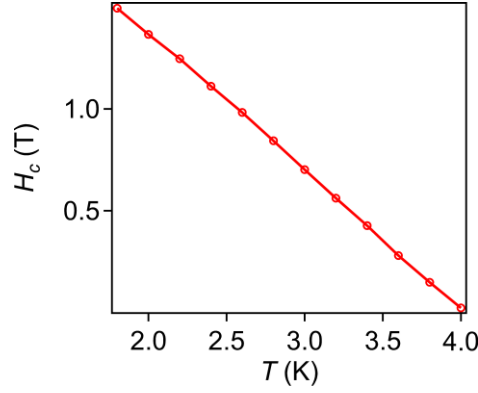


Fig. S3: Out-of-plane critical field vs temperature for a typical V device. The coherence length is estimated to be ~ 11 nm.

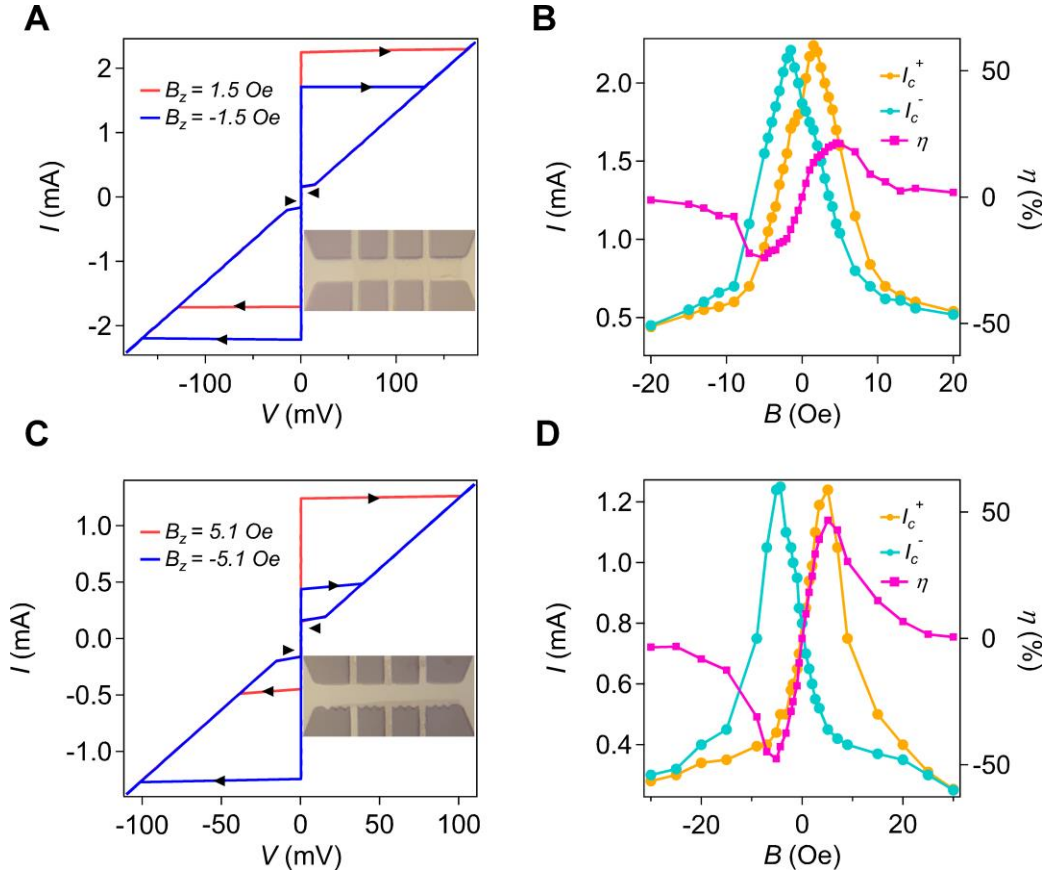


Fig. S4: Type A SC diode effect in V devices without and with defined edge asymmetry at 1.8 K. **a**, I - V scans of a V device without defined edge asymmetry at 1.5 Oe out-of-plane field along $\pm z$ direction as indicated by the red and blue lines. Black arrows show the scan direction. **b**, Critical currents and diode efficiency as a function of the magnetic field. **c-d**, Similar effects in the V device with one serrated edge and one 'straight' edge. Insets show the device image (dark areas on the devices are PMMA residuals).

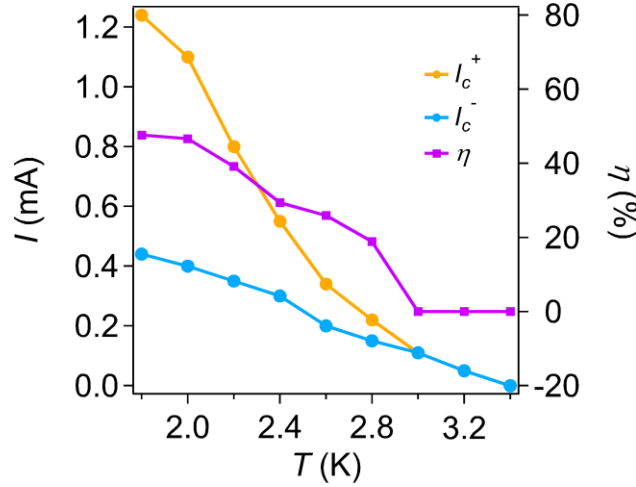


Fig. S5: Critical currents and diode efficiency of the device with defined edge asymmetry shown in Fig. S4C at different temperatures.

Note 1: Suppression of critical current by out-of-plane magnetic field.

In this section we give a physical explanation of why a very small perpendicular field can suppress the critical current by giving a simple derivation of the field B_s defined in the text.

The key observation is that in a thin film, the supercurrent is confined to a plane and is ineffective in screening an external field applied perpendicular to the plane. This problem was treated by Pearl (ref. 30) who showed that the field penetrates on the scale of the Pearl length $\lambda_p = \frac{2\lambda^2}{d}$ which greatly exceeds the usual London penetration depth λ . First, we consider the case when the sample width $W \ll \lambda_p$. This was the case treated by Maksimova (ref. 29). In this case the applied field penetrates completely. In the London gauge the vector potential $A_x = B_y$ and equals $\frac{BW}{2}$ at the sample edge. We use the London equation $j_s = \frac{c}{4\pi} \frac{A_x}{\lambda^2} = \frac{c}{8\pi} \frac{BW}{\lambda^2}$. Setting j_s to equal the Ginzburg-Landau critical current j_{GL} given by equation (8) in the text, we find the critical field to be $\frac{2}{3} \phi_0 / (\sqrt{3}\pi \xi W)$, which apart from the factor $\frac{2}{3}$, is the same as $B_s = \phi_0 / (\sqrt{3}\pi \xi W)$ quoted in the main text and in ref. 30.

In the opposite case $W \gg \lambda_p$, the field is confined to a distance equal to the Pearl length near the edge. Using equation (6) the vector potential A_x in the London gauge is found to be $B\lambda_p$ at the sample edge instead of $\frac{BW}{2}$ for the previous case. We can repeat the argument above but replace $\frac{W}{2}$ by λ_p . Therefore, in the expression for B_s we simply replace $\frac{W}{2}$ by λ_p in this limit.

Note 2: Precise removal of the out-of-plane magnetic field

To completely remove the out-of-plane component of the magnetic field, we measured the device in a dilution fridge fitted with a vector magnetic field configuration, where magnetic fields along two orthogonal directions B_1 and B_2 could be tuned individually. The device was mounted in a scheme shown in Fig. S6, where B_1 was along the device y axis ($B_1 = B_{1y}$), with some inevitable residual angle θ that created a small perpendicular component B_{1z} . This residual out-of-plane component was subsequently removed by adjusting B_2 along the z axis. Note that the offset angle θ in Fig. S6 is exaggerated for better illustration and the real angle is less than 1° .

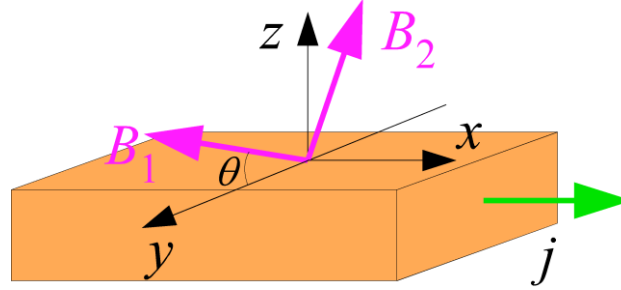


Fig. S6: Schematic depict of the device in a vector magnetic field. B_1 and B_2 are two individually adjustable magnetic fields orthogonal to each other. The device is placed so that B_1 is nominally in the film plane and perpendicular to the current flow direction. θ denotes the residual angle deviating from the film plane. This creates the residual out-of-plane component $B_{1z} = B_1 \sin \theta$, which is then eliminated by adjusting the second magnetic field B_2 along the z axis.

At each applied in-plane field, $B_2 = B_{2z}$ was scanned and critical currents of the device were measured. Figure S7 A shows I_c^\pm as a function of B_2 at different B_1 values. We found that while I_c^\pm vs B_2 always follows the inversed “V” shape, the peak position “ B_{2p} ” was shifted away from 0 when an in-plane field B_1 was applied. Further analysis shows that B_{2p} follows B_1 linearly (Fig. S7 B). This is reasonable because when an “in-plane” field B_1 is applied, the out-of-plane component B_{1z} suppresses the critical currents of the device. As B_2 is scanned along the z axis, the largest critical currents are located at where B_2 balances out B_{1z} ($B_2 = -B_{1z} = -B_1 \sin \theta$).

The residual angle θ for this device was then determined to be 0.291° by a linear fitting. With this information, we defined a corrected out-of-plane field $B_{zc} = B_2 + B_1 \times \sin 0.291^\circ$, which represents the actual out-of-plane magnetic field. Fig. S7 C-E present the critical current as a function of B_{zc} with the in-plane fields B_1 being 0 T, 2 T and 4 T, respectively. At $B_1 = 0$ T, a typical type A SC diode effect was observed, with the diode efficiency being 0 at $B_{zc} = 0$ Oe (Fig. S7 C). However, when the applied in-plane field was

2 T and 4 T, a clear difference between I_c^+ and I_c^- was observed even at $B_{zc} = 0$ Oe. Because the out-of-plane field is precisely 0, we attribute the observed supercurrent rectification at $B_{zc} = 0$ Oe to the effect of the actual in-plane magnetic field.

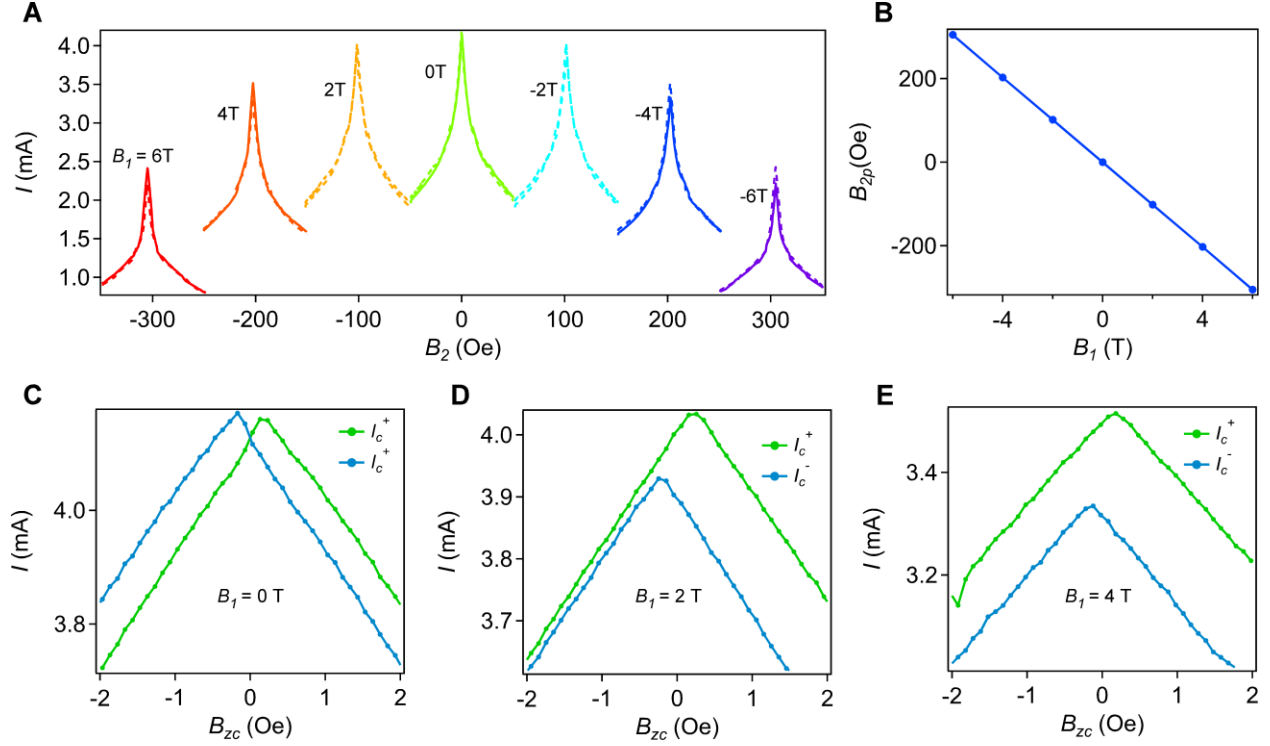


Fig. S7: Elimination of the out-of-plane magnetic field. (A) Critical currents vs B_2 at different values of B_1 for the scheme shown in Fig. S6. (B) Peak position of the critical current B_{2p} as a function of the applied in-plane field B_1 . (C-E) Critical currents vs corrected $B_{zc} = B_2 + B_1 \sin \theta$ showing actual in-plane field induced diode effect (type B). All data were measured at $T = 500$ mK.

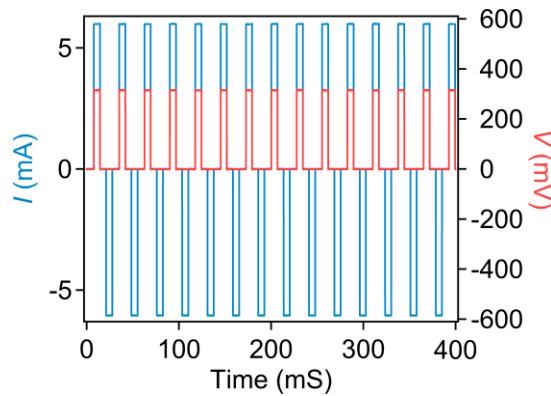


Fig. S8: Demonstration of a clear supercurrent rectification at $B_y = 200$ Oe and $T = 1$ K. The device current (blue) and the voltage drop (red) as a function of time is shown. The device behaved as a

superconductor supporting dissipationless current along the $-x$ direction, while dissipative current flows through a normal metal in the other direction.

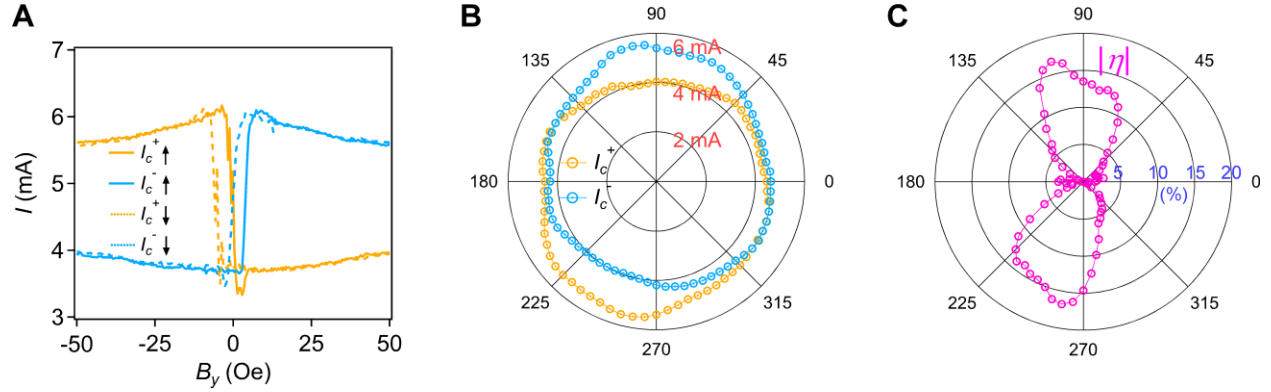


Fig. S9: Magnetic field and angle dependence of the diode effect for the second V/EuS device. (A) Magnetic field dependence of the critical currents at 1K. Solid (dashed) lines were obtained when scanning the magnetic field up (down). (B) Angle (ϕ) dependence of I_c^\pm at $T = 1$ K and $B_y = 50$ Oe. (C) The corresponding diode efficiency as a function of angle ϕ .